

SCIENTIFIC REPORTS



OPEN

East Asian Winter Monsoon Impacts the ENSO-related Teleconnections and North American Seasonal Air Temperature Prediction

Tianjiao Ma^{1,2}, Wen Chen^{1,2}, Debashis Nath¹, Hans-F. Graf¹, Lin Wang¹ & Jingliang Huangfu¹

El Niño–Southern Oscillation (ENSO) is a key feature for seasonal weather and climate prediction in the extra-tropics since related sea surface temperature anomalies induce precipitation anomalies that generate poleward propagating Rossby waves and teleconnections. The East Asian winter monsoon (EAWM) is driven by processes originating over the Asian continent and, to a lesser degree, by ENSO-related tropical convection. EAWM also strongly affects convection and precipitation patterns over the western tropical Pacific by cold air outbreaks reaching equatorial latitudes. Hence, one can expect a modulating effect of EAWM on the generation of Rossby wave trains related to ENSO. By increasing the convective heating over the western Pacific, strong EAWM strengthens the Pacific Walker circulation, and weakens (strengthens) the El Niño (La Niña) related effects on the extra-tropics via a modulation of the Pacific North America teleconnection pattern. Our results indicate that, for seasonal prediction over North America, along with ENSO the variability of EAWM should also be taken into account. The climate anomalies over the North America for the same phase of ENSO are significantly different for strong and weak EAWM.

El Niño–Southern Oscillation (ENSO) is the dominant interannual mode of climate variability in the tropical Pacific Ocean¹. During an El Niño event, increased rainfall and intensified convection dominates the tropical central-eastern Pacific, while dry conditions prevail in the tropical western Pacific² (Fig. 1a). The resulting anomalous diabatic forcing of the atmosphere, associated with ENSO, can affect the mid and high latitudes via atmospheric teleconnections^{3–7}. This makes ENSO the most important predictor for global seasonal climatic anomalies⁸.

The East Asian winter monsoon (EAWM) system is characterized by a cold-core Siberian High, a warm-core Aleutian Low, and a predominant low-level northeasterly wind blowing from East Asia to the low latitudes in the western Pacific Ocean^{9,10}. The EAWM can cause deep convection over the Maritime Continent, due to the intrusion of cold air into the tropics¹¹, which is even linked to the Australian summer monsoon¹². As a consequence, the East Asian Hadley circulation and the Walker circulations (the Indian and the Pacific Ocean cells) are intensified by the enhanced convective activity associated with the cold air outbreak events^{13,14}. The EAWM links interannual climatic anomalies from the mid and high latitudes of the East Asian region to the tropical western Pacific Ocean¹⁴ which is one of the key heating centers driving the tropical atmospheric circulations. On the other hand, ENSO strongly impacts tropical climate variability at the interannual time scale. Therefore, it is of great interest to understand what degree the EAWM modulates the ENSO-related atmospheric forcing along the equatorial Pacific Ocean and how this may affect the extra-tropical weather and climate.

There are suggestions that ENSO has an influence on EAWM^{15,16}, but the statistical evidence is weak (Table 1 shows roughly equal numbers of strong and weak EAWM for both, El Niño and La Niña, see also ref.^{17,18}). The influence of the EAWM on ENSO at an interannual time scale so far has received much less attention. To evaluate the ENSO independent variability of the EAWM system, we follow the methodology proposed by Chen *et al.*¹⁷. They separate the variability of the EAWM into two parts: the EAWM_{EN} and the EAWM_{res}. The

¹Center for Monsoon System Research, Institute of Atmospheric Physics, Chinese Academy of Sciences, Beijing, 100190, China. ²School of Earth Science, University of Chinese Academy of Sciences, Beijing, 100049, China. Correspondence and requests for materials should be addressed to W.C. (email: cw@post.iap.ac.cn)

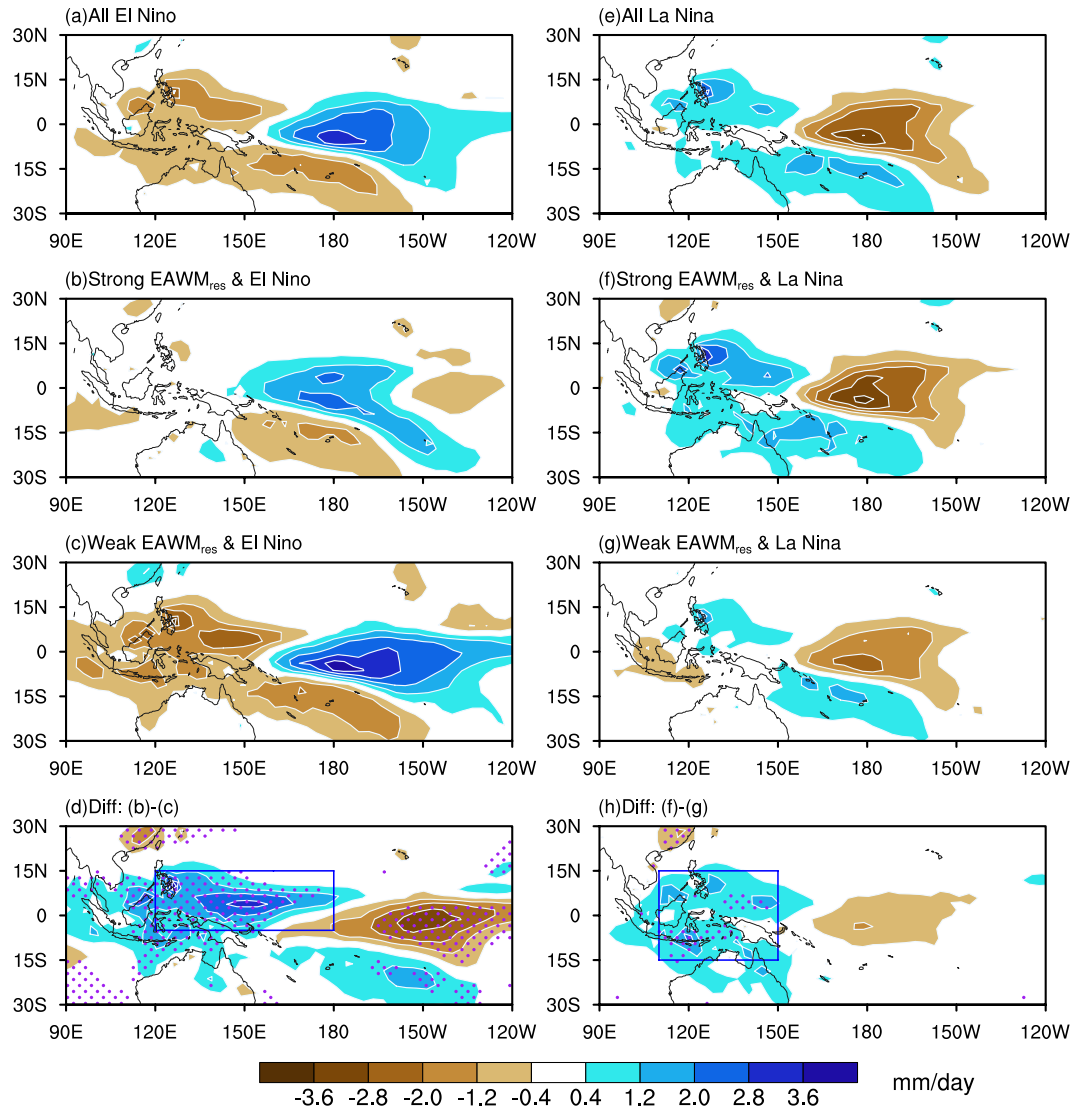


Figure 1. Composite winter mean (DJF) rainfall anomalies (Units: mm/day) in groups of: **(a)** mix of all El Niño events; **(b)** strong EAWM_{res}-El Niño; **(c)** weak EAWM_{res}-El Niño; **(d)** the difference between **(b)** and **(c)**; **(e)** mix of all La Niña events; **(f)** strong EAWM_{res}-La Niña; **(g)** weak EAWM_{res}-La Niña; and **(h)** the difference between **(f)** and **(g)**. Regions shaded with purple dots in **(d)** and **(h)** indicate the 90% confidence level. The maps in the figure are generated using the NCAR Command Language (NCL) (Version 6.4.0 & URL: <http://www.ncl.ucar.edu/Download/>).

EAWM_{EN} represents the variability of the EAWM which is correlated with the phases of ENSO. The EAWM_{res} is the ENSO-uncorrelated residual part, arising mainly from the internal processes of EAWM and the mid and high latitude processes over the Asian landmass. The EAWM_{res} and EAWM_{EN} accounts for ~87% and 13% of the total EAWM variability, respectively, which clearly indicates the dominance of the extratropical processes. Corresponding to a weak EAWM_{res}, anomalous low-level circulations are featured by decreased northerlies over East Asia, a weakened Aleutian low and an enhanced western North Pacific anticyclone¹⁷. It should be noted that the linear regression technique cannot fully separate the independent influences of ENSO and the EAWM. However, the linear regression is a common approach in many of the previous studies^{19,20}, and generally works because of little sea surface temperature (SST) anomalies in the tropics related to the EAWM_{res}¹⁷.

The causal linkage between the ENSO events and interannual precipitation anomalies in the tropics is well reported^{4,21}. However, the variability of tropical precipitation anomalies in the same phase of ENSO but under different extratropical circulation conditions is still not known. There is growing evidence that the extratropics can play an important role in ENSO evolution²²⁻²⁵. The primary objective of our present analysis is to investigate how and to what degree EAWM_{res} modulates the ENSO-SST related rainfall anomalies in the tropics. This study is of potential global significance, because the associated local or regional convective heating differences may trigger varied tropical-extratropical teleconnections due to poleward propagating Rossby waves being excited at different locations and with different strength.

Groups	years	CAO Frequency	CAO Strength
Strong EAWM _{res} -El Niño	[1953 1970 ^{EP} 1977 ^{EP} 1978 ^{CP} 1987 ^{EP} 2015 ^{CP}]	5.8**	0.6**
Weak EAWM _{res} -El Niño	[1954 1959 ^{CP} 1964 ^{CP} 1969 ^{CP} 1980 ^{CP} 1998 ^{EP} 2005 2010 ^{CP} 2016 ^{EP}]	3.3**	-0.2**
Strong EAWM _{res} -La Niña	[1956 1965 ^{EP} 1968 ^{EP} 1974 ^{CP} 1996 ^{EP} 1999 ^{CP} 2011 ^{CP}]	5.3*	0.7**
Weak EAWM _{res} -La Niña	[1950 ^{EP} 1972 ^{CP} 1975 ^{EP} 1976 ^{EP} 1985 ^{EP} 1989 ^{CP} 2001 ^{CP}]	4.0*	-0.1**

Table 1. Distribution of the ENSO events based on the EAWM_{res}, Cold Air Outbreak (CAO) frequency (times/winter) and interannual CAO strength index (normalized) in each group. Years 1953 indicate the winter mean of December 1952 to February 1953. The superscripts of EP (CP) indicate the Eastern (Central) Pacific type of ENSO. The double asterisk in the two El Niño groups (rows 1&2) denotes that the difference of CAO frequency (CAO strength) between the two El Niño groups exceeds the 95% (95%) one-tailed confidence level. The single (double) asterisk in the two La Niña groups (rows 3&4) indicates that the difference of CAO frequency (CAO strength) between the two groups of La Niña exceeds the 90% (95%) one-tailed confidence level, respectively.

Firstly, we present the composite rainfall anomalies over the Pacific Ocean under different background conditions as listed in Table 1 to show the modulating effect of the EAWM_{res} on the ENSO-related rainfall anomaly patterns in the tropical Pacific Ocean. Secondly, we illustrate the background atmospheric circulation conditions responsible for these rainfall anomalies over the Pacific Ocean. Thirdly, since the variability of ENSO has far-reaching impact on weather and climate over North America, we investigate how the EAWM_{res} is modulating the ENSO-related teleconnections and seasonal temperature anomaly patterns.

Results

SST related precipitation anomaly pattern modulated by EAWM_{res}. The influence of EAWM_{res} on the ENSO-induced tropical rainfall anomalies during boreal winter months is shown in Fig. 1. The left panel displays the mean rainfall anomalies during El Niño conditions. A composite from 25 El Niño events, Fig. 1a, is plotted for the purpose of comparison. We observe an increase in rainfall over the central and eastern Pacific, while drier conditions prevail over the western Pacific. These results are consistent with the previous studies⁴. Next, we sorted the El Niño events into strong and weak EAWM_{res} conditions (Table 1). It should be noted that the subgroups of ENSO events have no bias against the ENSO intensity or spatial pattern changes. The intensity of SST anomalies in the Niño3.4 region (5°N–5°S, 120°–170°W) shows a roughly even distribution regardless of the EAWM_{res} status (see Section Methods and supplementary Figure S1). Furthermore, the two types of ENSO events^{26,27} have no obvious preference in any of the subgroups as shown in Table 1. It is also confirmed from the SST anomaly patterns for each of the four subgroups of ENSO that neither of them shows any consistent bias towards a central Pacific or an eastern Pacific type (supplementary Figure S2). SST anomalies in the weak EAWM_{res}-El Niño are larger than those of the strong EAWM_{res}-El Niño, but their differences are statistically insignificant. This could be attributed to the top 2 strongest El Niño events (1997/98, 2015/16) in the former subgroup.

The precipitation anomalies during the two subgroups of El Niño show obvious differences in amplitude and spatial extents. In the strong EAWM_{res}-El Niño group, the below-normal (≤ -1.2 mm/day) rainfall is restricted to small regions near the Philippines, and west of Indonesia, whereas for the weak EAWM_{res}-El Niño group (Fig. 1c), drier conditions prevail over the entire western Pacific, the Maritime Continent and northern Australia. The daily average rainfall anomalies reach as low as -2.8 mm/day over the region between 0–15°N and 110°E–155°E. During the strong EAWM_{res}-El Niño years, the eastern edge of the “wetter than normal” region in the northern hemisphere is confined to a region south of Hawaii in the central-eastern Pacific, while during the weak EAWM_{res}-El Niño years it can extend further eastward to 120°W. The differences in rainfall anomalies between the strong and weak EAWM_{res}-El Niño years are shown in Fig. 1d. Clearly the modulating effect of EAWM_{res} on the El Niño-related rainfall anomalies in the tropics can be observed. It is characterized by a positive center over the western and negative over the eastern Pacific Ocean. The anomaly ranges between ± 2 –3 mm/day, the same magnitude of mean El Niño-related anomalies. Hence, the EAWM_{res} is playing an important role in modulating the El Niño-induced rainfall anomalies over the tropical Pacific Ocean. The stronger the EAWM_{res} is, the weaker is the relationship between El Niño and tropical rainfall anomalies, and vice versa for weak EAWM_{res}.

The right panel of Fig. 1 is similar, but for the La Niña conditions. Unlike for the El Niño conditions, the rainfall anomaly increases over the western Pacific Ocean, but decreases over the central equatorial Pacific Ocean (Fig. 1e). Strong EAWM_{res} under La Niña conditions brings heavier precipitation over the Philippines, the Maritime Continent and northern Australia (Fig. 1f). In contrast, weak EAWM_{res} under La Niña conditions favors abnormally low rainfall and drier conditions prevail in western Indonesia. The situation is very different over the central-eastern Pacific Ocean. Unlike during El Niño conditions, the EAWM_{res} couples only weakly with the tropical rainfall anomalies during La Niña conditions (Fig. 1h). On the one hand, this may be explained by the smaller amplitude of SST anomalies associated with La Niña. On the other hand, this may be attributed to La Niña related low SST over central-eastern Pacific and the threshold value (27–28 °C) for the occurrence of convection. Therefore, the EAWM_{res} has diverse influence on the ENSO-SST induced rainfall anomalies over the tropical Pacific Ocean.

The tropical rainfall anomaly patterns discussed above can be reconfirmed by several approaches. Firstly, as the subgroups have small numbers of samples for the composite analysis, we reconfirm our results using other datasets. The ECMWF’s 20th century (ERA20C) atmospheric reanalysis and Climatic Research Unit (CRU) time-series (TS) version 4.00 precipitation data are employed for larger samples. The common time period in the two datasets is 1900–2010, and the years for each of the categories are listed in supplementary Table S1. Although

limited by land precipitation only, results from these two longer datasets (supplementary Figure S3) are consistent with Fig. 1. Negative rainfall anomalies over the majority of the Maritime Continent during an El Niño are diminished by a strong $EAWM_{res}$ and enhanced by a weak $EAWM_{res}$. Similarly, Borneo, east Sumatra, and Java experience more rainfall during strong $EAWM_{res}$ -La Niña condition compared to that in weak $EAWM_{res}$ -La Niña condition. Secondly, results from the NOAA 20th Century reanalysis datasets are largely consistent with the former ones (supplementary Figure S4 and Table S2). Note that supplementary Figure S4 shows little significance over the central equatorial Pacific Ocean, and this could be attributed to the uncertainty in the reconstructed precipitation dataset which have large ensemble spread over the tropical central Pacific Ocean. Thirdly, we employed different EAWM indices^{28,29} to get the ENSO-unrelated residual EAWM part. The variability of these “ $EAWM_{res}$ ” yields very similar rainfall anomaly patterns as presented in Fig. 1 (figures not shown).

Possible mechanism. The Indo-Pacific Walker circulation is affected by both ENSO- and EAWM-related rainfall anomalies³⁰. In Fig. 2, anomalies of the Pacific Walker circulation are shown for all ENSO events and the different combinations of ENSO and $EAWM_{res}$ (Table 1) as anomalies of the 200hPa divergent wind and velocity potential. The variation of the Pacific Walker cell is closely tied to the zonal SST gradient anomalies between the central and western equatorial Pacific. However, it is noteworthy that the difference of zonal equatorial Pacific SST gradient in the two El Niño (La Niña) subgroups is statistically insignificant (see section Methods). Climatologically, during an El Niño event, the weaker zonal thermal and pressure gradients weaken the Walker cell (Fig. 2a), as seen by anomalous ascending motion over the central-eastern Pacific Ocean and descending motion over the Maritime Continent (Fig. 2a). Stronger $EAWM_{res}$ tends to weaken the Walker circulation anomalies initiated by the El Niño (Fig. 2b) i.e. convergence over the Maritime Continent has weakened to half the strength of its counterpart in the El Niño case. Figure 2c reflects the combined effect of weak $EAWM_{res}$ and the El Niño, resulting in a much stronger western-Pacific convergence and eastern-Pacific divergence. During the La Niña episodes (Fig. 2e), the anomalous Walker circulation behaves contrastingly, with anomalous ascending (descending) motions over the tropical western (central) Pacific Ocean. The divergent center over western Pacific extends southwestward during the strong $EAWM_{res}$ -La Niña case, whereas, it shrinks northward during the weak $EAWM_{res}$ -La Niña case. As a consequence, convergence of air masses over the tropical central-eastern Pacific is strengthened (weakened) by stronger (weaker) $EAWM_{res}$. It should be noted that the difference of Walker circulation anomalies between the strong and weak $EAWM_{res}$ cases is weak during the La Niña events (Fig. 2h). This could be attributed to the suppressed convections in the central-eastern Pacific Ocean during a La Niña event. In other words, La Niña-related negative SST anomalies superimposed on the climatological cold tongue would greatly decrease the occurrence of deep convection. That means the $EAWM_{res}$ would have limited impacts on tropical central-eastern Pacific during a La Niña event. What's more, the smaller amplitude of SST anomalies associated with La Niña may also explain the weak difference of the Walker cell. In general, the variability of the Walker Circulation shown in Fig. 2 is resulting in the aforementioned rainfall anomalies including the asymmetry between the El Niño and La Niña events (Fig. 1).

Previous studies^{13,14} reported that the cold air outbreaks (hereafter CAOs, also called cold surges) can trigger deep convective activity in the tropics. The CAOs are dominant feature of EAWM, which usually start with an intensification of Siberian-Mongolian High. Vigorous northerlies along the eastern flank of the Siberian-Mongolian high lead to a sharp rise in sea level pressure and sudden drop in surface temperature over East Asian region. When the CAO progresses rapidly southward, a frontal system of high pressure and near surface strong northerly winds affects the tropics. These induce low-level convergence and cyclonic vorticity over the tropical western Pacific sea surface. Hence, vertical lifting associated with the low-level convergence and cyclonic anomalies contribute to deep convection and heavy rainfall during the penetration of CAOs¹¹. Diabatic heating associated with the precipitation further accelerates both the local East Asian Hadley cell and the Walker cells over the Indian and Pacific Ocean¹⁴. Therefore, the mid-high latitude originated CAOs could affect the convections over tropics.

We plotted the outgoing longwave radiation (OLR) in Fig. 3a as a proxy of tropical Pacific convective activity associated with the $EAWM_{res}$. Due to the short time coverage of OLR dataset (1979–2016), we present the composite differences between strong and weak $EAWM_{res}$ during all ENSO years without separating further into El Niño or La Niña cases. As the weak $EAWM_{res}$ group contains more El Niño than La Niña events, weighted average is used to remove an El Niño bias. Similar averaging is performed for the strong $EAWM_{res}$ group prior to the analysis. Clearly, strong $EAWM_{res}$ favors enhanced convective activity over the tropical western Pacific and suppressed convective activity over the eastern Pacific Ocean (around 150°W). In Table 1 the frequency and strength of the cold air outbreaks in each of the subgroups is listed, indicating that strong $EAWM_{res}$ intensifies the CAO activity, and vice versa during weak $EAWM_{res}$. Thus, stronger $EAWM_{res}$ with intensified CAO activity triggers enhanced convective activity over the Maritime Continent. The related diabatic heating anomalies associated with convection are the key to the Pacific Walker circulation variability (Fig. 3b). In general, strong $EAWM_{res}$ triggers above-normal convective heating anomalies over the western Pacific Ocean, enhancing the climatological Walker circulation. It counteracts the El Niño-induced weakened Walker circulation anomalies, but amplifies the La Niña-induced enhanced anomalies over the tropical Pacific Ocean. The situation is opposite but weaker during weak $EAWM_{res}$, when the El Niño-induced weakened Walker circulation is amplified and the anomalies due to La Niña are suppressed.

The rainfall variability over the tropical western Pacific Ocean in response to ENSO was suggested to be directly related to the low-level circulation anomalies around the Philippines^{15,16}. However, the cyclonic/anticyclonic flow over this region also has a close connection with the $EAWM_{res}$. Feng and Chen¹⁸ reported that during an El Niño event, the Philippine anticyclone tends to be weak (strong) in presence of a strong (weak) $EAWM_{res}$, and vice versa during the La Niña years (see ref.¹⁸ Figs 4, 5). Furthermore, according to the numerical experiments by Feng *et al.*³¹, during an El Niño event the negative convective heating anomaly around the Maritime

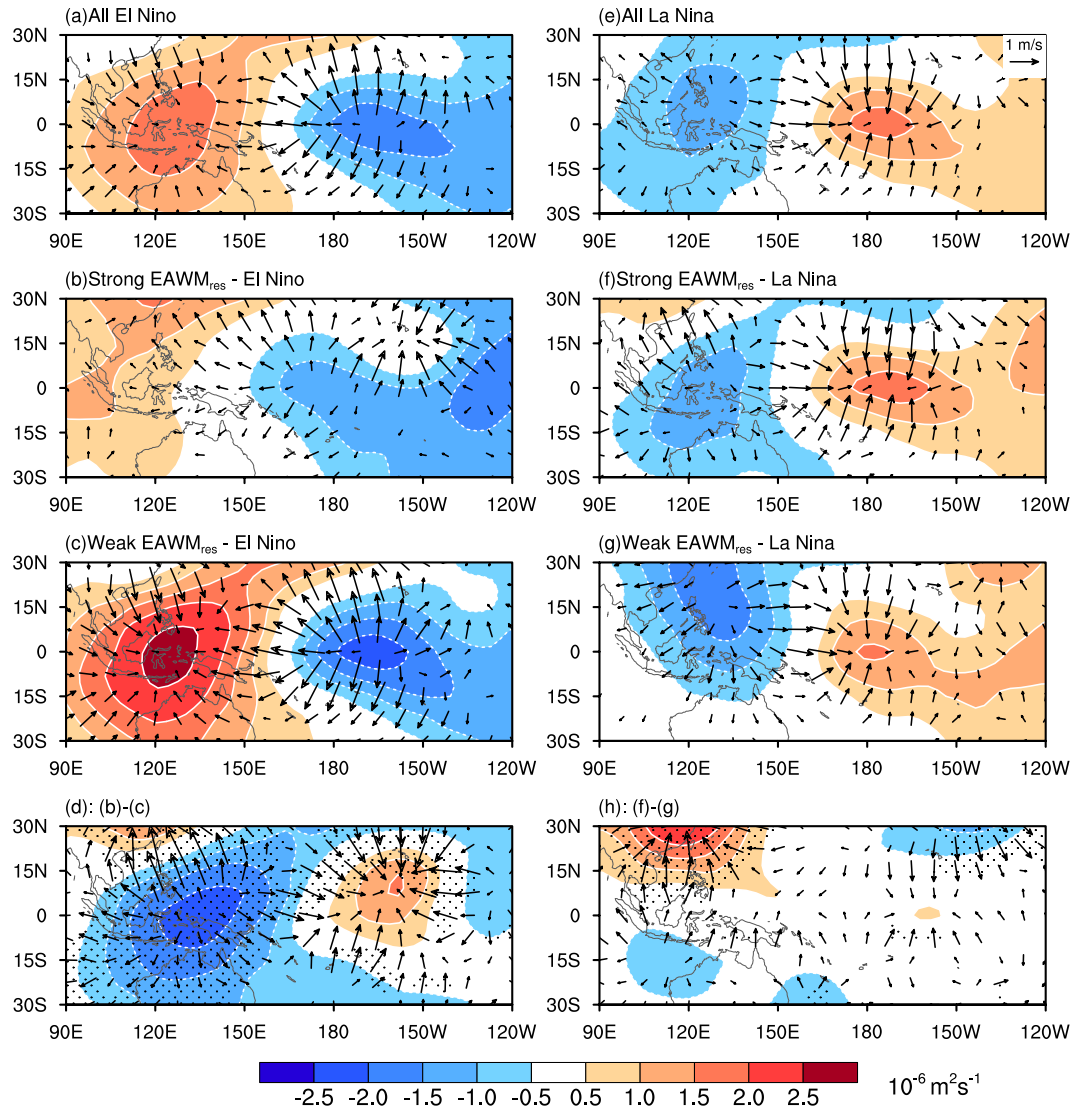


Figure 2. As in Fig. 1, but for 200-hPa divergent winds (vectors; m s^{-1}) and velocity potential (contours; $10^{-6} \text{ m}^2 \text{ s}^{-1}$). Regions shaded with black dots in (d) and (h) indicate that either the divergent winds or velocity potential are significant at the 90% confidence level. The maps in the figure are generated using the NCAR Command Language (NCL) (Version 6.4.0 & URL: <http://www.ncl.ucar.edu/Download/>).

Continent plays a dominant role for the existence of the Philippine anticyclone. Positive convective diabatic heating anomalies during strong EAWM_{res} balance the El Niño-related Maritime Continent negative heating anomalies, which weakens the Philippine anticyclone. On the other hand, convective cooling during weak EAWM_{res} strengthens the Philippine anticyclone, and vice versa for the La Niña. Thus, in the western Pacific the EAWM_{res} modulates the ENSO-related rainfall anomalies, mediated by the variation of low-level Philippine anticyclone.

The EAWM_{res} has diverse impacts on the ENSO-related tropical rainfall anomalies in the warm and cold phases: First, the EAWM_{res} has a weaker modulation effect during the La Niña than the El Niño events. Such asymmetric behavior is consistent with the fact that rainfall anomalies have a saturation effect in La Niña but more intense in the El Niño conditions³². Second, a stronger EAWM_{res} amplifies the rainfall anomalies over the region $5^{\circ}\text{S}–15^{\circ}\text{N}$, $120^{\circ}\text{E}–180^{\circ}\text{E}$ under El Niño (Fig. 1d) and $15^{\circ}\text{S}–15^{\circ}\text{N}$, $110^{\circ}\text{E}–150^{\circ}\text{E}$ under La Niña (Fig. 1h) conditions, respectively. The southwestward tilt in the precipitation anomaly pattern during La Niña conditions is in line with the trajectories of the cold air outbreaking events¹⁶. The Siberian High and the Aleutian Low experience a systematic eastward and westward shift in El Niño and in La Niña winters, respectively¹⁶. Hence, during El Niño cold air outbreaking events are more frequent across the Philippines. In contrast, during La Niña conditions cold air outbreaking events are shifted westward to the Sunda Strait¹⁶.

Impacts on the US air temperature forecast. ENSO is reported to have significant impact on climate in the mid and high latitudes, particularly over the North America through the Pacific–North American (PNA) teleconnection pattern³³. The longitudinal shift in the PNA pattern, due to the movement of the driving diabatic heating centers, is resulting in different climatic anomalies over North America³⁴. Considering these complex

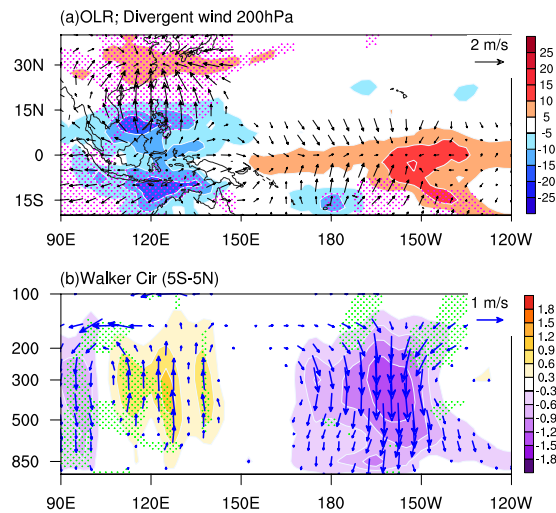


Figure 3. (a) Difference between strong and weak EAWM_{res} during the ENSO years: Outgoing Longwave Radiation (OLR; color filling, unit: W/m^2); divergent winds at 200hPa (vector). The time period is 1979–2016 due to the short coverage of OLR dataset. (b) Difference of tropical omega (color filling) and zonal Walker circulation (vector) for average of 5°S–5°N between strong and weak EAWM_{res} during the ENSO years. The original omega (unit: Pa/s) is multiplied by -100.0 so that positive values indicate upward motion. Regions shaded with dots indicate the 90% confidence level. The maps in the figure are generated using the NCAR Command Language (NCL) (Version 6.4.0 & URL: <http://www.ncl.ucar.edu/Download/>).

interactions, it is interesting to investigate whether EAWM_{res} is modulating the ENSO-related climate anomalies (e.g. air temperature) over the North America. During the El Niño winter months, often the southern part of the United States (US) experiences colder than normal conditions, whereas the northern part of North American are warmer. The situation is just opposite during the La Niña winters (Fig. 4a and e). Taking also the information of EAWM_{res} into account, the North American air temperature anomalies display quite different patterns: the strong EAWM_{res}-El Niño case is favoring a southeast (cold)-northwest (warm) contrast (Fig. 4b); weak EAWM_{res}-El Niño initiates warmer conditions in northeastern North American. These variabilities in air temperature anomalies are consistent with the shift in the PNA-like pattern (Fig. 4, purple lines), which is generated by the latent heating centers in the tropics^{27,34}. Stronger (Weaker) EAWM_{res}, with central (eastern) Pacific latent heating (induced by above-normal rainfall anomalies, Fig. 1b and c), powers the westward (eastward) shift of the PNA-like pattern and the air temperature anomalies over the North America. Besides, the strength of Aleutian Low over North Pacific during the strong and weak EAWM_{res} - El Niño is related to the combined effect of El Niño and EAWM_{res}. El Niño and strong EAWM_{res} contribute to an intensified Aleutian Low but weak EAWM_{res} acts opposite. Contrastingly, in the La Niña winters, the temperature difference between the two La Niña subgroups shows a quadrupole pattern, which is also consistent with the variation of 500 hPa geopotential height (Z500) (Fig. 4h). A wave train along Japan, west of Bering Sea, south to the Gulf of Alaska and eastern North Pacific is observed in Z500. The positive Z500 anomaly over Bering Sea and negative anomaly over Alaska favors stronger northerly winds between the two, which leads to a band of negative SAT over Alaska. Positive SAT anomalies over the western United States could be attributed to the southwesterly anomalies between the negative (north) and positive (southeast) Z500 anomalous centers over the eastern North Pacific. Results from a linear baroclinic model illustrated that the atmospheric linear response to an idealized western tropical Pacific thermal forcing is characterized by a wave train transporting from east of Japan to North America³⁵. The wave train pattern in the North Pacific sector in Fig. 4h is similar with the numerical results³⁵, implying that the precipitation anomalies over the tropical western Pacific accounts for the different distributions of Z500 and SAT anomalies during two subgroups of La Niña. Surface air temperature differences between strong and weak EAWM_{res} for similar ENSO conditions can vary by 1–2°C, which is comparable to the anomalies due to ENSO alone. This indicates that EAWM_{res} is an additional important factor which may interfere with the seasonal North American air temperature prediction.

Summary and Discussion

This study is mainly dedicated to a better understanding of the modulating effects of the EAWM_{res} on the ENSO-related rainfall and circulation variability in the tropics. Composite results suggest that a strong EAWM_{res} weakens the El Niño-induced Pacific rainfall and Walker circulation anomalies, while a weak EAWM_{res} amplifies them. A strong EAWM_{res} brings more cold air outbreaks to the low-latitudes. It intensifies the tropical deep convection and diabatic heating over the western Pacific. On the one hand, the anomalous heating weakens the low-level Philippine anticyclone and diminishes the consequent negative rainfall anomalies during the El Niño. On the other hand, the strong EAWM_{res} induced western Pacific heating, pumps the Pacific Walker circulation in a positive feedback loop. Over the eastern Pacific the stronger Pacific Walker circulation favors stronger surface divergence and less rainfall. Weak EAWM_{res}, with below-normal heating anomalies over the western Pacific, will

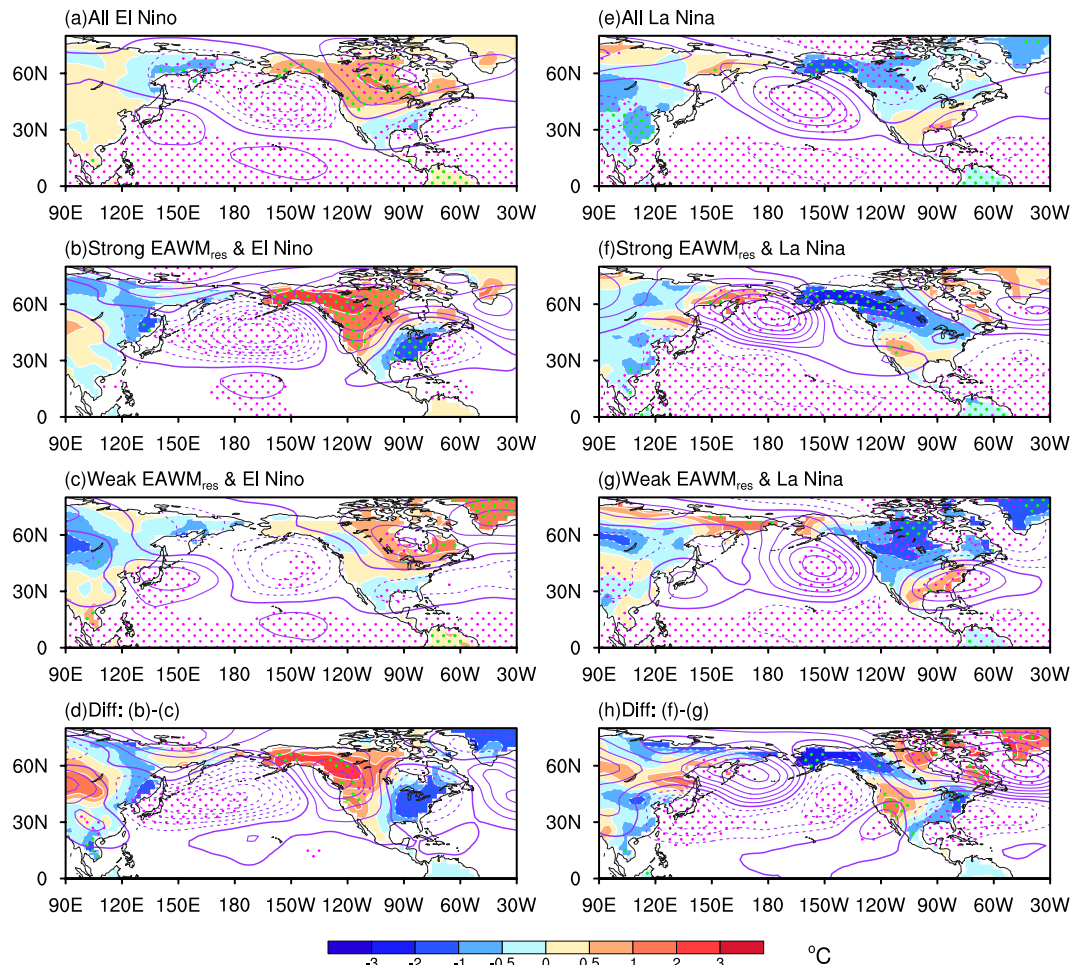


Figure 4. As in Fig. 1, but for winter-mean North American surface air temperature anomalies (color) and 500 hPa geopotential height anomalies (purple lines, CI = 10 gpm, zero line is bolded). Purple and green dots indicate that the HGT500 and SAT anomalies exceed 90% confidence levels, respectively. The maps in the figure are generated using the NCAR Command Language (NCL) (Version 6.4.0 & URL: <http://www.ncl.ucar.edu/Download/>).

amplify the anomalies related to the El Niño. A similar $EAWM_{res}$ intervention can be seen during the La Niña events. However, the $EAWM_{res}$ appears to have a small contribution to the eastern Pacific rainfall due to the cold SST anomalies over there inhibiting convective rainfall anyway. Through its impact on West Pacific rainfall and the Pacific Walker cell, the $EAWM_{res}$ also affects the ENSO-related temperature variability over the North America. Strong $EAWM_{res}$ warms the western part and cools the eastern part of North America during an El Niño, whereas it cools the northwestern edge of North America and warms the western part of US during a La Niña. ENSO, thus, is not the only potential predictor for North American seasonal forecasts; the $EAWM$ is similarly important and should be accounted for in the future.

The stratification of ENSO events into four subgroups lead to small sample sizes, and one may concern about the robustness of the composite. Hence, we add some supplementary analysis. As mentioned in results section (a), more samples (listed in supplementary Table S1) are obtained by using datasets which cover a longer period, the ERA20C atmospheric reanalysis and CRU data. Besides precipitation (supplementary Figure S3), composite anomalies of Walker cell and Z500, SAT (supplementary Figures S5, 6) are consistent with the former results in Figs 2 and 4, respectively.

Methods

Datasets. The National Centers for Environmental Prediction - National Center for Atmospheric Research (NCEP-NCAR) monthly mean atmospheric reanalysis data³⁶ are used in this study. This datasets have a horizontal resolution of 2.5° latitudes by 2.5° longitudes, 17 levels in the vertical direction, and a time period of 1948-present. For sea surface temperature (SST) we used the $1.0^\circ \times 1.0^\circ$ horizontal resolution monthly mean Hadley Centre Global Sea Ice and Sea Surface Temperature (HadISST) dataset³⁷. The HadISST data covers the time period from 1870 to the present. In addition, for rainfall data we employed the globally gridded ($2.5^\circ \times 2.5^\circ$) monthly-mean NOAA Precipitation Reconstruction (PREC) data from 1948 to the present³⁸. The NOAA Outgoing Longwave Radiation (OLR)³⁹ data, available from 1979 to 2016, is used to signal the activities of convection.

We use the data averaged from December to February to represent boreal winter mean. The analysis period spans from 1948 to 2016, except for that related with OLR (from 1979 to 2016). Conventionally, the winter of

1949 refers to the December 1948 to February 1949. All the original datasets are subjected to a 7-year high pass Lanczos filter to suppress the decadal variability. Moreover, we also use the monthly mean 20th century reanalysis datasets⁴⁰ (from 1851 to 2012), ERA-20C reanalysis datasets⁴¹ (from 1900 to 2010), Climate Research Unit (CRU) Time-Series (TS) version 4.00 gridded temperature and precipitation data⁴² (from 1901 to 2015), and the NOAA Extended Reconstructed Sea Surface Temperature (ERSST) V4 (1854-present)^{43,44} to compare our results.

Indices and methods. The EAWM_{res} index¹⁷, which represents the interannual variability of EAWM_{res}, is calculated by removing the ENSO-related part by linear regression. The original EAWM_{res} index is multiplied with -1 , so that a positive index corresponds to northerly winds and a strong EAWM_{res} state. Strong (Weak) EAWM_{res} winters are selected based on a threshold of $+(-) 0.5$ standard deviations of EAWMI_{res}. We then obtain 20 strong and 20 weak EAWM_{res} winters over the period of 1948–2016, respectively.

The Oceanic Niño index (ONI), which is defined by the Climate Prediction Center (CPC) as the 3-month running mean of ERAAT.v4 SST anomalies in the Niño-3.4 region (5°N – 5°S , 120°W – 170°W), is used as an ENSO index here. According to the CPC, when the $\pm 0.5^{\circ}\text{C}$ threshold of ONI is met for a minimum of 5 consecutive overlapping months, it can be recognized as an El Niño/La Niña event. Based on these criteria, we obtain 25 El Niño and 20 La Niña events from the 69 winters between 1948 and 2016. ENSO events after 1950 are obtained from the CPC website <http://www.cpc.ncep.noaa.gov>. The ENSO events are further sorted into 4 groups based on different conditions of EAWM_{res}.

- 1) Strong EAWM_{res} with El Niño
- 2) Weak EAWM_{res} with El Niño
- 3) Strong EAWM_{res} with La Niña
- 4) Weak EAWM_{res} with La Niña

All these selected years are listed in Table 1. It should be noted that the oceanic Niño index (ONI) is linearly independent of the EAWM_{res} index. And the intensity of ENSO events shows a roughly even distribution regardless of the EAWM_{res} status (supplementary Figure S1).

Eastern-Pacific (EP) and Central-Pacific (CP) ENSO events are identified by normalized winter mean Niño 3 index and El Niño Modoki index (EMI)²⁶. When the normalized EMI exceeds 0.7 (-0.7), meanwhile greater (less) than the normalized Niño 3 index, a CP El Niño (La Niña) is defined. In the same way, an EP El Niño (La Niña) is identified when the normalized Niño 3 index greater (less) than 0.7 and also greater (less) than the EMI. Years that both of the two Niño indices don't exceed a 0.7 standard deviation would not be classified to any type. Thus, two types of ENSO are separated as listed in Table 1.

The zonal SST gradient along the equatorial Pacific Ocean between the central and western Pacific is defined as the difference in area averaged SST between the Niño 4 (160°E – 150°W , 5°S – 5°N) region and the western Pacific Ocean (90° – 150°E , 5°S – 5°N). Result of 1000 bootstrapping⁴⁵ combinations shows that the zonal SST gradient difference between the strong EAWM_{res}-El Niño group and the weak EAWM_{res}-El Niño group (the strong EAWM_{res}-La Niña group and the weak EAWM_{res}-La Niña group) is insignificant at the 90% confidence level based on a two-tailed test. The result is same if considering the zonal SST gradient between the eastern (Niño3 region, 150°W – 90°W , 5°S – 5°N) and the western equatorial Pacific.

Cold Air Outbreak. The winter frequency of CAO events is obtained from Abdillah⁴⁶ (Figure A2; W-CAO over East Asian; period 1958–2013). Table 1 listed the average winter frequency of East Asian CAO events in each group. As the samples sizes are small, we used the bootstrap method⁴⁵, resampling 1000 times, and one-tailed test to estimate the mean differences from two samples. The winter frequency of CAO events in the strong EAWM_{res}-El Niño group is significantly higher than that in the weak EAWM_{res}-El Niño group at a confidence level of 95%. Between the two groups during the La Niña, the difference reaches the 90% confidence level.

We adopt an alternative approach to estimate the interannual variation of CAOs. A profound characteristic related with CAOs in the tropics is the disturbance of sea level pressure (SLP)^{13,14}. Usually, the time scale of a CAO event is about 5 days⁴⁷, therefore a 3–6 day band pass filter is applied on the SLP anomaly over the western tropical Pacific region to define the East Asian cold air outbreaking events. Thus, an annual CAO strength index is defined as an area-averaged variance of the filtered anomalies during winter in the region between 0 – 15°N and 105°E – 125°E . We checked the robustness of the index by considering smaller and bigger areas, however, the result remains the same. The average strength of the CAO strength index (normalized) is -0.1 for El Niño (25 events) and 0.1 for La Niña (18 events) conditions, reflecting the influence of ENSO on cold surges⁴⁶. But when we include the EAWM_{res} variability, the CAO strength index for the strong EAWM_{res} groups is much higher than for the weak EAWM_{res} groups. The values are 0.6 & -0.2 for El Niño and 0.7 & -0.1 for La Niña, respectively. The difference of CAO strength indices between the strong EAWM_{res}-El Niño (La Niña) group and the weak EAWM_{res}-El Niño (La Niña) group exceed the 95% (95%) confidence level according to a one-tail bootstrap statistical estimate. This indicates that strong EAWM_{res} intensify the CAO activities, and vice versa during weak EAWM_{res}, regardless of El Niño or La Niña background.

Divergent wind calculation. The horizontal wind can be divided into two components: non-divergent (or rotational) and divergent wind⁴⁸.

$$\vec{V} = \vec{V}_{\psi} + \vec{V}_{\chi} \quad (1)$$

In equation (1), ψ represents stream function and χ represents velocity potential.

$$u_{\psi} = -\frac{\partial\psi}{\partial y}, v_{\psi} = \frac{\partial\psi}{\partial x} \quad (2)$$

$$u_{\chi} = \frac{\partial\chi}{\partial x}, v_{\chi} = \frac{\partial\chi}{\partial y} \quad (3)$$

In equations (2) and (3), u_{ψ} , v_{ψ} stand for the rotational components of horizontal wind and u_{χ} , v_{χ} represent the divergent wind. The horizontal divergence (D) is calculated by

$$D = \nabla \cdot \vec{V} = \nabla \cdot \vec{V}_{\psi} + \nabla \cdot \vec{V}_{\chi} = \nabla \cdot \vec{V}_{\chi} \quad (4)$$

Hence, substituting equations (3) into (4) yields

$$D = \frac{\partial^2\chi}{\partial x^2} + \frac{\partial^2\chi}{\partial y^2} \quad (5)$$

Therefore, velocity potential χ can be obtained by solving the Poisson equation according to the equation, then u_{χ} , v_{χ} can be obtained via equation (3).

References

- Rasmusson, E. M. & Carpenter, T. H. Variations in tropical sea surface temperature and surface wind fields associated with the Southern Oscillation/El Niño. *Mon. Weath. Rev.* **110**, 354–384 (1982).
- Trenberth, K. E. & Caron, J. M. The Southern Oscillation revisited: Sea level pressures, surface temperatures, and precipitation. *J. Clim.* **13**, 4358–4365 (2000).
- Horel, J. D. & Wallace, J. M. Planetary-scale atmospheric phenomena associated with the Southern Oscillation. *Mon. Weath. Rev.* **109**, 813–829 (1981).
- Ropelewski, C. F. & Halpert, M. S. Global and regional scale precipitation patterns associated with the El Niño/Southern Oscillation. *Mon. Weath. Rev.* **115**, 1606–1626 (1987).
- Gershunov, A. & Barnett, T. P. Interdecadal modulation of ENSO teleconnections. *Bull. Amer. Meteor. Soc.* **79**, 2715–2725 (1998).
- Zhou, W. & Chan, J. C. ENSO and the South China Sea summer monsoon onset. *Int. J. Climatol.* **27**, 157–167 (2007).
- Jia, X., Ge, J. & Wang, S. Diverse impacts of ENSO on wintertime rainfall over the Maritime Continent. *Int. J. Climatol.* **36**, 3384–3397 (2016).
- Larkin, N. & Harrison. Global seasonal temperature and precipitation anomalies during El Niño autumn and winter. *Geophys. Res. Lett.* **32**, L16705, <https://doi.org/10.1029/2005GL022860> (2005).
- Chen, W., Graf, H. & Huang, R. The interannual variability of East Asian Winter Monsoon and its relation to the summer monsoon. *Adv. Atmos. Sci.* **17**, 48–60 (2000).
- Wang, B. *The Asian Monsoon*. 89–110 (Springer, 2006).
- Chang, C. P. *et al.* The Global Monsoon System: Research and Forecast 2nd Edition. 85–110 (World Scientific, 2011).
- Eroglu, D. *et al.* See-saw relationship of the Holocene East Asian–Australian summer monsoon. *Nat. Commun.* **7**, 12929, <https://doi.org/10.1038/ncomms12929> (2016).
- Chang, C. P. & Lau, K. Northeasterly cold surges and near-equatorial disturbances over the winter MONEX area during December 1974. Part II: Planetary-scale aspects. *Mon. Weath. Rev.* **108**, 298–312 (1980).
- Compo, G., Kiladis, G. & Webster, P. The horizontal and vertical structure of East Asian winter monsoon pressure surges. *Quart. J. Roy. Meteor. Soc.* **125**, 29–54 (1999).
- Zhang, R., Sumi, A. & Kimoto, M. Impact of El Niño on the East Asian monsoon: A diagnostic study of the '86/87 and '91/92 events. *J. Meteor. Soc. Japan.* **74**, 49–62 (1996).
- Wang, B., Wu, R. & Fu, X. Pacific–East Asian teleconnection: how does ENSO affect East Asian climate? *J. Clim.* **13**, 1517–1536 (2000).
- Chen, W., Feng, J. & Wu, R. Roles of ENSO and PDO in the Link of the East Asian Winter Monsoon to the following Summer Monsoon. *J. Clim.* **26**, 622–635 (2013).
- Feng, J. & Chen, W. Interference of the East Asian winter monsoon in the impact of ENSO on the East Asian summer monsoon in decaying phases. *Adv. Atmos. Sci.* **31**, 344–354 (2014).
- Wu, R., Chen, W., Wang, G. & Hu, K. Relative contribution of ENSO and East Asian winter monsoon to the South China Sea SST anomalies during ENSO decaying years. *J. Geophys. Res. Atmospheres.* **119**, 5046–5064 (2014).
- Zhou, L. & Wu, R. Respective impacts of the East Asian winter monsoon and ENSO on winter rainfall in China. *J. Geophys. Res. Atmospheres* **115**, D02107, <https://doi.org/10.1029/2009JD012502> (2010).
- Huang, P. & Xie, S.-P. Mechanisms of change in ENSO-induced tropical Pacific rainfall variability in a warming climate. *Nature Geos.* **8**, 922–926 (2015).
- Vimont, B. & Hirst. The seasonal footprinting mechanism in the CSIRO general circulation models. *J. Clim.* **16**, 2653–2667 (2003).
- Wang, S.-Y., L'Heureux, M. & Chia, H.-H. ENSO prediction one year in advance using western North Pacific sea surface temperatures. *Geophys. Res. Lett.* **39**, <https://doi.org/10.1029/2012GL050909> (2012).
- Boschat, G., Terray, P. & Masson, S. Extratropical forcing of ENSO. *Geophys. Res. Lett.* **40**, 1605–1611 (2013).
- Chen, S., Chen, W., Yu, B. & Graf, H.-F. Modulation of the seasonal footprinting mechanism by the boreal spring Arctic Oscillation. *Geophys. Res. Lett.* **40**, 6384–6389 (2013).
- Weng, H., Behera, S. K. & Yamagata, T. Anomalous winter climate conditions in the Pacific rim during recent El Niño Modoki and El Niño events. *Clim. Dyn.* **32**, 663–674, <https://doi.org/10.1007/s00382-008-0394-6> (2009).
- Feng, J., Chen, W. & Li, Y. Asymmetry of the winter extra-tropical teleconnections in the Northern Hemisphere associated with two types of ENSO. *Clim. Dyn.* **48**, 2135–2151 (2016).
- Chen, Z., Wu, R. & Chen, W. Distinguishing Interannual Variations of the Northern and Southern Modes of the East Asian Winter Monsoon. *J. Clim.* **27**, 835–851 (2014).
- Li, Y. & Yang, S. A Dynamical Index for the East Asian Winter Monsoon. *J. Clim.* **23**, 4255–4262 (2010).
- Webster, P. J. *et al.* Monsoons: Processes, predictability, and the prospects for prediction. *J. Geophys. Res.* **103**, 14451–14510 (1998).
- Feng, J., Wang, L., Chen, W., Fong, S. & Leong, K. Different impacts of two types of Pacific Ocean warming on Southeast Asian rainfall during boreal winter. *J. Geophys. Res.* **115**, D24122, <https://doi.org/10.1029/2010JD014761> (2010).
- Hoerling, K. & Z. El Niño, La Niña, and the nonlinearity of their teleconnections. *J. Clim.* **10**, 1769–1785 (1997).

33. Kumar & Hoerling. Annual cycle of Pacific–North American seasonal predictability associated with different phases of ENSO. *J. Clim.* **11**(12), 3295–3308 (1998).
34. Simmons, A. J., Wallace, J. M. & Branstator, G. W. Barotropic wave propagation and instability, and atmospheric teleconnection patterns. *J. Atmos. Sci.* **40**, 1363–1392 (1983).
35. Jia, X., Wang, S., Lin, H. & Bao, Q. A connection between the tropical Pacific Ocean and the winter climate in the Asian-Pacific region. *J. Geophys. Res.* **120**, 430–448, <https://doi.org/10.1002/2014JD022324> (2015).
36. Kalnay, E. *et al.* The NCEP/NCAR 40-year reanalysis project. *Bull. Amer. Meteorol. Soc.* **77**, 437–471 (1996).
37. Rayner, N. *et al.* Global analyses of sea surface temperature, sea ice, and night marine air temperature since the late nineteenth century. *J. Geophys. Res. Atmospheres* **108**, <https://doi.org/10.1029/2002JD002670> (2003).
38. Chen, M., Xie, P., Janowiak, J. E. & Arkin, P. A. Global land precipitation: A 50-yr monthly analysis based on gauge observations. *J. Hydrometeorol.* **3**, 249–266 (2002).
39. Lee, H-T. Climate Algorithm Theoretical Basis Document (C-ATBD): Outgoing Longwave Radiation (OLR) - Daily. NOAA's Climate Data Record (CDR) Program, CDRP-ATBD-0526, 46 pp (2014).
40. Compo, G. P. *et al.* The twentieth century reanalysis project. *Q. J. R. Meteorol. Soc.* **137**, 1–28 (2011).
41. Poli, P. *et al.* ERA-20C: An atmospheric reanalysis of the twentieth century. *J. Clim.* **29**, 4083–4097 (2016).
42. University of East Anglia Climatic Research Unit; Harris, I.C.; Jones, P.D. CRU TS4.00: Climatic Research Unit (CRU) Time-Series (TS) version 4.00 of high-resolution gridded data of month-by-month variation in climate (Jan. 1901–Dec. 2015). Centre for Environmental Data Analysis, (2017).
43. Huang, B. *et al.* Extended reconstructed sea surface temperature version 4 (ERSST.v4). Part I: upgrades and intercomparisons. *J. Clim.* **28**, 911–930 (2015).
44. Liu, W. *et al.* Extended reconstructed sea surface temperature version 4 (ERSST.v4): part II. Parametric and structural uncertainty estimations. *J. Clim.* **28**, 931–951 (2015).
45. Efron, B. & Tibshirani, R. An introduction to the bootstrap. (1993)
46. Abdillah, M., Kanno, Y. & Iwasaki, T. Tropical–Extratropical Interactions Associated with East Asian Cold Air Outbreaks. Part I: Interannual Variability. *J. Clim.* <https://doi.org/10.1175/jcli-d-16-0152.1> (2017)
47. Shoji, T., Kanno, Y., Iwasaki, T. & Takaya, K. An Isentropic Analysis of the Temporal Evolution of East Asian Cold Air Outbreaks. *J. Clim.* **27**, 9337–9348 (2014).
48. Krishnamurti, T. N. Tropical east-west circulations during the northern summer. *J. Atmos. Sci.* **28**, 1342–1347 (1971).

Acknowledgements

This work is supported jointly by the National Natural Science Foundation of China (Grant No. 41721004), the Chinese Academy of Sciences Key Research Program of Frontier Sciences (QYZDY-SSW-DQC024) and “The Belt and Road Initiatives” Program on International Cooperation: Climate Change Research and Observation Project (134111KY5B20160010). We are also thankful to the agencies which provide us the datasets for our analysis. The NCEP Reanalysis Derived data, Precipitation reconstruction dataset (PREC), OLR data, 20th Century Reanalysis V2c data, and NOAA_ERSST_V4 data are provided by the NOAA/OAR/ESRL PSD, Boulder, Colorado, USA, from their web site at <http://www.esrl.noaa.gov/psd/>. The CRU data are provided by the Centre for Environmental Data Analysis from their web site <http://catalogue.ceda.ac.uk>. ERA-20C dataset is obtained from the web site of ECMWF at <https://www.ecmwf.int>. Hans-F. Graf is a Visiting Fellow of the Chinese Academy of Sciences.

Author Contributions

W.C. designed the research. T.M. performed the analysis. W.C., T.M. and D.N. wrote the paper. H-F.G. contributed to improving the analysis and interpretation. All authors discussed the results and commented on the manuscript.

Additional Information

Supplementary information accompanies this paper at <https://doi.org/10.1038/s41598-018-24552-3>.

Competing Interests: The authors declare no competing interests.

Publisher's note: Springer Nature remains neutral with regard to jurisdictional claims in published maps and institutional affiliations.



Open Access This article is licensed under a Creative Commons Attribution 4.0 International License, which permits use, sharing, adaptation, distribution and reproduction in any medium or format, as long as you give appropriate credit to the original author(s) and the source, provide a link to the Creative Commons license, and indicate if changes were made. The images or other third party material in this article are included in the article's Creative Commons license, unless indicated otherwise in a credit line to the material. If material is not included in the article's Creative Commons license and your intended use is not permitted by statutory regulation or exceeds the permitted use, you will need to obtain permission directly from the copyright holder. To view a copy of this license, visit <http://creativecommons.org/licenses/by/4.0/>.

© The Author(s) 2018